Brain Imaging and Behavior
DOI 10.1007/s11682-017-9681-3

ORIGINAL RESEARCH

Brain white matter structural networks in patients with non-neuropsychiatric systemic lupus erythematosus

Ling Zhao[1] · Xiangliang Tan[2] · Junjing Wang[1] · Kai Han[3] · Meiqi Niu[1] · Jun Xu[4] · Xiaojin Liu[1] · Xixi Zhao[2] · Miao Zhong[1] · Qin Huang[5] · Yikai Xu[2] · Ruiwang Huang[1]

© Springer Science+Business Media New York 2017

Abstract Previous neuroimaging studies have revealed cognitive dysfunction in patients with systemic lupus erythematosus (SLE) and suggested that it may be related to disrupted brain white matter (WM) connectivity. However, no study has examined the topological properties of brain WM structural networks in SLE patients, especially in patients with non-neuropsychiatric SLE (non-NPSLE). In this study, we acquired DTI datasets from 28 non-NPSLE patients and 24 healthy controls, constructed their brain WM structural networks by using a deterministic fiber tracking approach, estimated the topological parameters of their structural networks, and compared their group differences. We reached the following results: 1) At the global level, the non-NPSLE patients showed significantly increased characteristic path length, normalized clustering coefficient and small-worldness, but significantly decreased global efficiency and local efficiency compared to the controls; 2) At the nodal level, the non-NPSLE patients had significantly decreased nodal efficiency in regions related to movement control, executive control, and working memory (bilateral precentral gyri, bilateral middle frontal gyri, bilateral inferior parietal lobes, left median cingulate gyrus and paracingulate gyrus, and right middle temporal gyrus). In addition, to pinpointing the injured WM fiber tracts in the non-NPSLE patients, we reconstructed the major brain WM pathways connecting the abnormal regions at the nodal level with the corticospinal tract (CST), superior longitudinal fasciculus-parietal terminations (SLFP), and superior longitudinal fasciculus-temporal terminations (SLFT). By analyzing the diffusion parameters along these WM fiber pathways, we detected abnormal diffusion parameters in the bilateral CST and right SLFT in the non-NPSLE patients. These results seem to indicate that injured brain WM connectivity exists in SLE patients even in the absence of neuropsychiatric symptoms.

Keywords Diffusion tensor imaging (DTI) · Fractional anisotropy (FA) · Fronto-parietal network · Working memory network

Highlights: 1. Revealed altered global parameters of brain WM structural networks in non-NPSLE patients.
2. Detected decreased nodal efficiency in the sensorimotor and fronto-parietal networks in non-NPSLE patients.
3. Found abnormal diffusion parameters in the bilateral CST and right SLFT in non-NPSLE patients.
4. Observed reconfiguration of hub regions in non-NPSLE patients relative to healthy subjects.

Ling Zhao and Xiangliang Tan contributed equally to this work.

Electronic supplementary material The online version of this article (doi:10.1007/s11682-017-9681-3) contains supplementary material, which is available to authorized users.

✉ Yikai Xu
yikaivip@163.com

✉ Ruiwang Huang
ruiwang.huang@gmail.com

[1] Center for the Study of Applied Psychology, School of Psychology, Key Laboratory of Mental Health and Cognitive Science of Guangdong Province, Brain Study Institute, South China Normal University, Guangzhou 510631, People's Republic of China

[2] Department of Medical Imaging Center, Nanfang Hospital, Southern Medical University, Guangzhou 510515, People's Republic of China

[3] Department of Dermatology, Nanfang Hospital, Southern Medical University, Guangzhou 510515, People's Republic of China

[4] Department of Hematology, Nanfang Hospital, Southern Medical University, Guangzhou 510515, People's Republic of China

[5] Department of Rheumatology, Nanfang Hospital, Southern Medical University, Guangzhou 510515, People's Republic of China

Published online: 11 February 2017

Abbreviations

DTI	diffusion tensor imaging;
SLE	systemic lupus erythematosus;
NPSLE	neuropsychiatric systemic lupus erythematosus;
non-NPSLE	non-neuropsychiatric systemic lupus erythematosus;
ACR	American College of Rheumatology;
SLEDAI	Systemic Lupus Erythematosus Disease Activity Index;
SLICC/ACR	Systemic Lupus International Collaborating Clinics/American College of Rheumatology Damage Index;
TRAUCULA	TRActs Constrained by UnderLying Anatomy algorithm;
CNS	central nervous system;
WM	white matter;
TBSS	Tract-Based Spatial Statistics;
FA	fractional anisotropy;
MD	mean diffusivity;
RD	radial diffusivity;
AD	axial diffusivity

Introduction

Systemic lupus erythematosus (SLE), a chronic relapsing-remitting and female-predominant autoimmune disease, is characterized by multisystem microvascular inflammation and even affects the central nervous systems (CNS) (Ercan et al. 2016). Mikdashi (2016) systematically reviewed previous fMRI studies and indicated that various cognitive functions, including motor control, executive function, working memory, attention, and language processing, have been impaired in SLE patients with and without neuropsychiatric symptoms (NPSLE and non-NPSLE). Previous studies reported that about 75% of SLE patients have cognitive impairment making it the most common symptom (Jeltsch-David and Muller 2014; Shapira-Lichter et al. 2016). Filley et al. (2009) analyzed the relationship between white matter (WM) microstructure changes and cognitive impairment in non-NPSLE patients and indicated that brain WM injury is involved in the initial disease progression of SLE, which may further lead to NPSLE. In fact, several studies indicated that brain WM injury may be an underlying mechanism of cognitive dysfunction in SLE (Elizabeth Kozora et al. 2008; Benedict et al. 2008; E Kozora et al. 2011). Therefore, an in-depth study of brain WM abnormalities may contribute to understanding how SLE affects the brain cognitive function and evolves into NPSLE.

Diffusion tensor imaging (DTI) is the only available non-invasive technique for studying brain WM microstructures and for mapping brain WM connectivity in vivo (Mori and Zhang 2006). Because NPSLE is accompanied by cognitive dysfunction and is related to high morbidity, high mortality, and poor prognosis, previous studies have tried to uncover the pathogenic mechanisms of the neuropsychological symptoms using DTI. Several studies have used DTI to detect brain WM abnormalities related to NPSLE on the basis of diffusion parameters (Emmer et al. 2010; Ercan et al. 2016). For example, Emmer et al. (2010) collected DTI datasets from 12 NPSLE patients and 28 healthy controls, measured the diffusion parameters of the water in the WM tracts using the Tract-Based Spatial Statistics (TBSS) method, and found significantly decreased fractional anisotropy (FA) in NPSLE patients compared to healthy controls. Ercan et al. (2016) also found significantly decreased FA and significantly increased mean diffusivity (MD) and radial diffusivity (RD) using the TBSS method in NPSLE patients compared to healthy controls. We noticed that NPSLE patients recruited in previous studies were a mixture of various neuropsychological symptoms, and usually accompanied by regional brain atrophy and WM lesions (Luyendijk et al. 2011; Appenzeller et al. 2008; Ercan et al. 2016), which may confound neuroimaging studies of NPSLE patients. Thus, to avoid those potential confounds, we selected the SLE patients, who did not show neuropsychiatric symptoms (non-NPSLE) or regional brain atrophy or WM lesions, as samples to identify brain structural alterations. This may help to better explain how SLE affects brain structure and induces future cognitive dysfunction. By now, very few studies (Ercan et al. 2016; Zimny et al. 2014) have explored brain WM structure abnormality in non-NPSLE patients.

The brain WM structural network has been increasingly applied to explore various neuropsychiatric disorders, including Alzheimer's disease (Daianu et al. 2015), multiple sclerosis (Li et al. 2013), and schizophrenia (Sun et al. 2015). Lin et al. (2011) analyzed the brain regional activity in non-NPSLE patients and found that SLE functional alterations may be related to intrinsic networks involving multiple brain areas. DiFrancesco et al. (2007) found abnormal brain activation patterns when childhood-onset SLE patients performed a series of cognitive tasks and suggested that the abnormal brain activation patterns of SLE may be related to brain WM connectivity abnormalities rather than to injury of specific gray matter areas. However, most previous studies focused on regional changes in the diffusion parameters in SLE patients and, as far as we have found, no study has directly investigated axonal connectivity per se in SLE patients from the perspective of brain WM structural networks.

With the goal of exploring the topological property alteration of WM structural networks in non-NPSLE patients, we acquired DTI datasets from 28 non-NPSLE patients and 24 healthy controls. After constructing their brain structural networks by using deterministic tractography, we estimated their topological parameters by using graph theory and compared

their between-group differences. In addition, to further pinpoint the injured WM fiber tracts in the non-NPSLE patients, we used the FreeSurfer/TRACULA tool to reconstruct the brain major WM pathways. Because WM injury has been found in non-NPSLE patients in previous studies (Shapira-Lichter et al. 2016; Filley et al. 2009), we hypothesized that the global and nodal parameters would be significantly changed in the non-NPSLE patients compared to the healthy controls and that the diffusion parameters of the major WM pathways would also be significantly different between the two groups.

Materials and methods

Subjects

Thirty-three female right-handed non-NPSLE patients were recruited from the Department of Rheumatology, Nanfang Hospital, Southern Medical University, Guangzhou, China. The inclusion criterion was that they must meet the SLE diagnostic criteria of the American College of Rheumatology (ACR) (Hochberg 1997) but without any neuropsychiatric syndromes (Liang et al. 1999). In order to increase the accuracy of the diagnosis, independent clinical diagnoses of non-NPSLE were made separately for the patients by a dermatologist (K. H.) and a rheumatologist (Q. H.). The disease activity index for each non-NPSLE patient was evaluated by the same rheumatologist (Q. H.) according to the Systemic Lupus Erythematosus Disease Activity Index (SLEDAI) (Brunner et al. 1999; Bombardier et al. 1992). The disease severity for each non-NPSLE patient was assessed using the Systemic Lupus International Collaborating Clinics/American College of Rheumatology (SLICC/ACR) Damage Index at the time of the MRI acquisition (Gladman et al. 1996). Other clinical indicators, including the age at onset (AAO), duration of illness (DOI), dosage of prednisone (DOP), and three serum assay indices (C3, C4, and CH50), were recorded for each patient (Table 1). The exclusion criteria for the patients were as follows: (1) ambidexterity, (2) current pregnancy, (3) a history of head trauma, (4) any history of alcohol/substance misuse, (5) symptoms of anxiety or depression, (6) a history of other neurological or psychiatric disorders, (7) other medical condition or treatment irrelevant to SLE but potentially affecting the brain, and (8) positive antiphospholipid antibodies, which are known to be related to cerebrovascular disease. In addition, we recruited 30 right-handed healthy female volunteers from the local community as the healthy controls. The exclusion criteria for the controls were same as those for the non-NPSLE patients. In addition, the healthy controls were not included if they had any history of an Axis-I psychiatric disorder or neurological disorder or had first-degree relatives with a psychotic disorder. The study protocol was approved by the Research Ethics Committee of Nanfang Hospital of the Southern Medical University. Written informed consent was obtained from each subject prior to this study. Table 1 lists the demographic information for all the patients and the controls.

Table 1 Demographic and clinical information for the patients with non-neuropsychiatric systemic lupus erythematosus (non-NPSLE) and the healthy controls (HC) in this study

Characteristics	non-NPSLE (n = 28)	HC (n = 24)	p-value
Female	28	24	
Age (years old)	30.5 ± 10.5 [18–50]	29.5 ± 7.70 [20–46]	0.71
SLICC	0.57 ± 0.57 [0–2]	NA	
SLEDAI	9.18 ± 6.80 [0–23]	NA	
AAO (years)	27.7 ± 11.1 [13–49]	NA	
DOI (months)	33.8 ± 49.7 [1–204]	NA	
DOP (mg/day)	38.1 ± 22.8 [10–100]	NA	
C3 (g/l)	0.62 ± 0.29 [0.22–1.25]	NA	
C4 (g/l)	0.11 ± 0.69 [0.01–0.29]	NA	
CH50 (g/l)	32.7 ± 19.9 [0.02–65.9]	NA	

A two-sample t-test was used to compare between-group differences ($p < 0.05$)

Abbreviations: *SLICC* Systemic Lupus International Collaborating Clinics/American College of Rheumatology Damage Index, *SLEDAI* Systemic Lupus Erythematosus Disease Activity Index, *AAO* Age at onset, *DOI* Duration of illness, *DOP* Dosage of prednisone, C3, C4, and CH50, three serum assay indices, *NA* not applicable

Image acquisition

All MRI data were collected at Nanfang Hospital on a 3 T Philips Achieva MR scanner with an 8-channel head coil. For each subject, foam pads were used to reduce head motion. The DTI data were acquired using a single-shot spin-echo diffusion-weighted EPI sequence with the following parameters: repetition time (TR) = 9950 ms, echo time (TE) = 86 ms, flip angle =90°, 32 non-collinear directions with b = 1000 s/mm^2, a volume without diffusion weighting (b_0), field of view (FOV) = 224 × 224 mm^2, data matrix =112 × 112, slice thickness = 2 mm without inter-slice gap, and 75 axial slices covering the whole brain. We also acquired high resolution brain structural images for each subject by using a T1-weighted 3D turbo field echo (TFE) sequence: TR = 9.0 ms, TE = 4.0 ms, flip angle =8°, FOV = 256 × 256 mm^2, data matrix =256 × 256, slice thickness = 1 mm, and 176 sagittal slices covering the whole brain. In addition, we used a T2-weighted fluid-attenuated inversion-recovery (FLAIR) sequence to collect the brain images, which were inspected by a radiologist (X. T.) to exclude any structural abnormalities, such as brain lesions, infarction, or atrophy, in any of the subjects.

Image quality

To assure the image quality, we first assessed the raw DTI data with a careful visual inspection. Three datasets (2 non-NPSLE patients and 1 healthy control) that had artifacts, ghosting, or incomplete scanned images were removed from the subsequent analyses. Then we estimated the head motion parameters in the raw DTI data because it is particularly sensitive to the subject's head motion and eddy currents (Yendiki et al. 2013).

Head motion during the DTI scanning will not only result in misalignment between the images in the series but can also alter the intensity of the images. Although a registration-based correction approach is often used in DTI studies, the deleterious effects of head motion cannot be fully eliminated (Yendiki et al. 2013). Previous studies (Koldewyn et al. 2014; Yendiki et al. 2013) demonstrated that significant group differences in head motion can be a serious confounding factor and can greatly affect the detection of differences in DTI measures. It has been suggested that the head motion effect can be ameliorated by including head motion parameters as a nuisance regressor in the analysis (Koldewyn et al. 2014; Yendiki et al. 2013). In this study, we processed the head motion parameters using the TRAUCULA (TRActs Constrained by UnderLying Anatomy) algorithm (Yendiki et al. 2011) implemented in FreeSurfer (http://surfer.nmr.mgh.harvard.edu/). We first applied an affine registration (Jenkinson et al. 2002) to reduce the misalignment between the images and accordingly reoriented the corresponding diffusion-weighting gradient vectors (Leemans and Jones 2009; Rohde et al. 2004). Then on the basis of the affine registration, we estimated four parameters, average volume -by-volume translation, average volume-by-volume rotation, percentage of slices with signal drop-out, and signal drop-out severity. The last two parameters are specific to DTI (Benner et al. 2011). Afterward, we calculated the total motion index (TMI) (Koldewyn et al. 2014; Yendiki et al. 2013) (see Supplementary Materials), which was used to quantify the diffusion image quality and used as a nuisance regressor.

Figure 1 shows the four DTI head motion parameters for all 60 subjects after checking the images. Considering the levels of the four head motion parameters, we excluded the unqualified images for 8 subjects (gray) (3 non-NPSLE patients and 5 controls) due to excessive head motion. Therefore, in the end, we included 28 non-NPSLE patients (28 females, aged 18–50 years old, 30.5 ± 10.5 years old) and 24 HC subjects (24 females, aged 20–46 years old, 29.5 ± 7.7 years old) for further analysis. The two groups were closely matched in the head motion measures (translation: $p = 0.87$, two-sample t-test; rotation: $p = 0.15$, two-sample t-test). The other two head motion measures, percentage of slices with signal drop-out and signal drop-out severity, equaled 0 and 1, respectively, for each of the subjects (Table S2).

Construction of brain structural networks

DTI data preprocessing

DTI data were preprocessed using the PANDA toolbox (http://www.nitrc.org/projects/panda). The preprocessing steps included: (1) extracting the brain mask, (2) cropping the non-brain space in the native images, (3) correcting for the eddy-current distortion and head motion by registering the diffusion-weighted images to the b_0 images with an affine

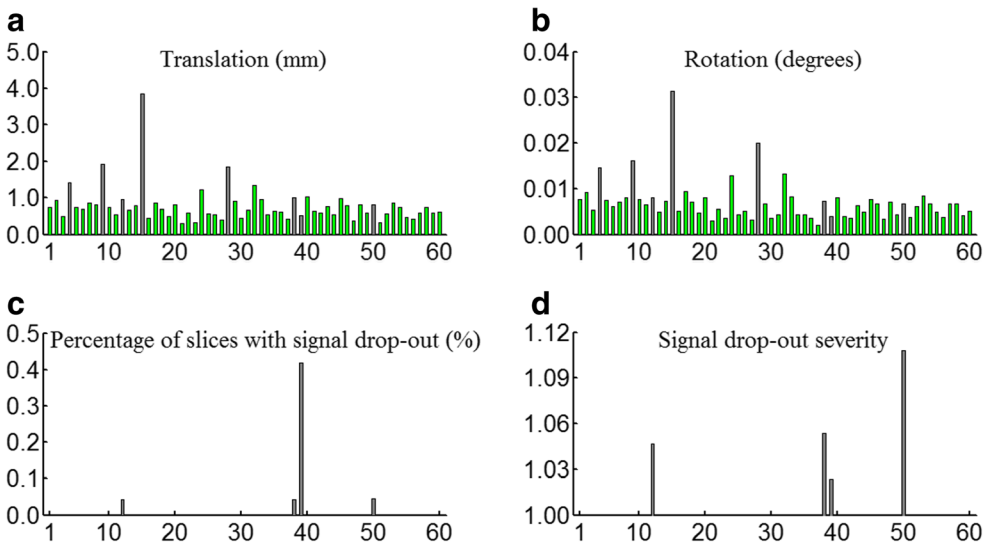

Fig. 1 Illustration of the four head motion parameters for the 60 subjects after visual inspection in this study. The vertical axes represent the four head motion parameters: **a** translation, average volume-by-volume translation; **b** rotation, average volume-by-volume rotation angles; **c** percentage of slices with signal drop-out; and **d** signal drop-out severity. The horizontal axis represents the index of the subjects. Eight subjects (*gray*) were excluded due to excessive motions after a comprehensive consideration of the above four parameters. The others, the remaining 52 subjects (*green*), were included in the subsequent analysis

transformation, and (4) estimating the diffusion tensor metrics using a linear least-squares fitting method.

Network construction

Network node definition The human brain structural network was constructed based on the automated structural labeling (AAL) template (Tzourio-Mazoyer et al. 2002), which parcellates the brain into 90 regions of interest (ROIs). Each ROI was defined as a node with detectable structural connection between each pair of nodes as an edge. The individual T1-weighted structural images were co-registered to its corresponding FA native diffusion space using an affine transformation. The individual transformed structural images were then normalized to the ICBM152 template in the MNI space using a nonlinear transformation (FSL/FNIRT). An inverse transformation was used to warp the AAL-90 template in the MNI space to the native diffusion space by a nearest-neighbor interpolation method (Gong et al. 2009; Wen et al. 2011). After data registration, PANDA can generate registration images for quality inspection, the registration images of each subject was carefully checked to make sure the registration and segmentation quality.

Network edge definition Whole-brain fiber tracking was performed in native diffusion space for each subject using the Fiber Assignment by Continuous Tracking (FACT) algorithm (Mori et al. 1999) embedded in the Diffusion Toolkit (http://www.trackvis.org/dtk/). To reconstruct the WM fibers, we drew streamlines from each voxel following the principal diffusive direction. Fiber tracking was terminated when the streamline reached a voxel with FA < 0.2 or when the fiber tract angle exceeded 45° between two consecutive voxels. Whole-brain fiber streamlines was rendering by TrackVis (http://www.trackvis.org/) (Fig. S1). The distribution of fiber streamlines could help to evaluate the quality of tractography. Following a previous study (Lo et al. 2010), we used the streamline number (*SN*) and *FA* to define the edge weight, i.e., $w_{ij} = FA \times SN$; that is, the edge weight was found by multiplying the *SN* by the mean *FA* along the inter-nodal streamlines that connected a pair of ROIs. To reduce the false-positive connections that resulted from noise (Lo et al. 2010), we defined a structural connection as existing between a pair of ROIs if $SN \geq 2$. Thus, a 90 × 90 symmetric weighted network was constructed for each subject. The flowchart for construction of the WM structural network is presented in Supplementary Materials (Fig. S2).

Network analysis

The topological properties of the human brain structural networks were analyzed using graph theory (Bullmore and Sporns 2009). We calculated both global and nodal parameters to describe the topological properties of the structural networks by using the GRETNA toolbox (http://www.nitrc.org/projects/gretna/). The global parameters included the clustering coefficient (C_p), shortest path length (L_p), global efficiency (E_{glob}), local efficiency (E_{loc}), normalized clustering coefficient (γ), normalized shortest path length (λ), and small-world parameters (σ). We also estimated the nodal parameters, specifically, the nodal efficiency (E_{nod}), nodal strength (S_{nod}) and betweenness centrality (*BC*). In addition, nodes were defined as hub nodes of a brain network if E_{nod} was at least one standard deviation (SD) greater than the average nodal efficiency of the group network (i.e., E_{nod} > mean + SD). The definitions and interpretations of these topological parameters are described in Table S1 (Supplementary Materials) and also can be found in Rubinov and Sporns (2010).

White matter pathways

By comparing between-group difference in the nodal parameters, we can identify abnormal brain regions in the non-NPSLE patients. In this study, the abnormal brain regions were primarily located in the bilateral precentral gyri (PreCG.L/R), bilateral middle frontal gyri (MFG.L/R), and bilateral inferior parietal lobes (IPL.L/R) (see Fig. 2 and Table 3), which are connected by the corticospinal tract

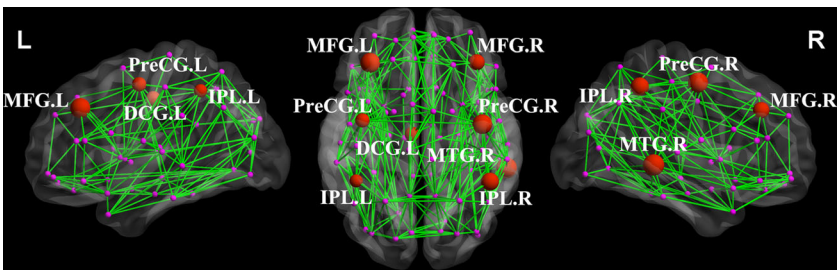

Fig. 2 Abnormal brain regions with altered nodal parameters in brain white matter structural networks in the patients with non-neuropsychiatric systemic lupus erythematosus (non-NPSLE) and the healthy controls (HC). The red nodes indicate that the nodal efficiency in the non-NPSLE patients was uniformly significantly decreased compared to the controls. The pink nodes indicate no significant between-group differences in the nodal efficiency. The size of the red nodes is proportion to the nodal efficiency value for the non-NPSLE patients. The brain networks, which were visualized using BrainNet Viewer software (http://www.nitrc.org/projects/bnv/), are for illustration purposes only. Abbreviations: PreCG, precentral gyrus; MFG, middle frontal gyrus; IPL, inferior parietal lobe; DCG, median cingulate and paracingulate gyri; and MTG, middle temporal gyrus

(CST), superior longitudinal fasciculus-parietal terminations (SLFP), and superior longitudinal fasciculus-temporal terminations (SLFT). To check the integrity of these WM tracts (CST, SLFP, and SLFT), we compared the between-group differences in the mean values of the fractional anisotropy (FA), mean diffusivity (MD), radial diffusivity (RD), and axial diffusivity (AD). First, we reconstructed the CST, SLFP, and SLFT using FreeSurfer/TRACULA, an automated global probabilistic tractography algorithm (Yendiki et al. 2011). Then after reconstruction of brain WM fibers, the volumetric distributions of diffusion parameters (FA, MD, RD, and AD) for each pathway were produced, and the distribution values of the FA, MD, RD, and AD in each voxel were weighted by the corresponding prior probability. The diffusive parameters were computed by thresholding the pathway distributions at 20% of their maximum value; thus the subsequent comparison of the parameters was based on the center of the distribution and not its tails.

Statistical analysis

Group effect analysis Two-sample *t*-tests were used to determine between-group differences in age and the head motion parameters. A nonparametric permutation test (Nichols and Holmes 2002) was used to determine significant between-group differences in the topological parameters of the brain structural networks and the mean diffusion parameters (i.e., FA, MD, RD, and AD) in the WM tracts. This permutation procedure was repeated 10,000 times to obtain an empirical distribution of the difference. We set the significance threshold at $p < 0.05$. In the statistical analysis, we took the age and TMI as nuisance regressors and regressed them out. The false discovery rate (FDR) approach was used to correct for multiple comparisons (Benjamini and Hochberg 1995).

Correlations between network parameters and clinical variables For the nodal parameters with a significant between-group difference, we computed the relationship between the nodal parameters of the abnormal brain regions and each of the clinical variables (i.e., AAO, DOI, DOP, SLICC, C3, C4, and CH50) by performing partial correlation analyses while controlling for age and TMI as confounding covariates. All of the statistical analyses were performed using SPSS 22.0. The significance level was set at $p < 0.05$.

Robustness of the network analysis

Robustness is a key issue in network analysis. In this study, we repeated the network analyses by considering different definitions of edges and nodes to check that the group differences in the topological parameters reflected true differences rather than artifacts.

Effect of streamline numbers False-positive or false-negative connections can result from the selection of the fiber connection numbers (Zhang et al. 2014; Bassett et al. 2011). To examine the robustness of the main results that we obtained using $w_{ij} = FA \times SN$ with the selected threshold of $SN \geq 2$ to define the edge weight, we also selected two additional thresholds, $SN \geq 1$ and $SN \geq 3$, to define the edge weight. In this way, we reconstructed the brain structural networks that corresponded to the newly selected thresholds and repeated the network analyses.

Effect of defining different edge weights Previous studies have used several different definitions of the edge weight in constructing the structural networks (Shu et al. 2011; Wen et al. 2011; Bassett et al. 2011). However, different definitions of edge weight may result in variability in the statistical analysis of the topological parameters of the structural networks (Zhong et al. 2015). To examine the robustness of the main results corresponding to the edge weight $w_{ij} = FA \times SN$, we selected an additional way to define edge weight, i.e., $w_{ij} = SN$. In these calculations, we took $w_{ij} = SN$ using three different thresholds of SN ($SN \geq 1$, $SN \geq 2$, and $SN \geq 3$) to examine the robustness of the main results.

Effects of brain parcellation Previous studies showed that statistical results for the network topological parameters may be related to different spatial resolutions of brain template (Fornito et al. 2010; Zalesky et al. 2010). Thus, we reconstructed the brain structural networks using the AAL-1024 template, a high-resolution brain template that randomly subdivides the AAL template into 1024 equal size regions (http://andrewzalesky.com/software.html). We repeated the network analysis and determined between-group differences in the network parameters using the same process as above.

Results

Demographic information and head motion measures

Table 1 lists the demographic information of the non-NPSLE patients and the healthy controls. No significant between-group differences were found in either sex (all female) or age ($p = 0.71$, two-sample *t*-test).

Global parameters

Table 2 lists the global parameters for both the non-NPSLE patients and the healthy controls. Compared to the controls, the patients had significantly increased δ ($p = 0.019$), γ ($p = 0.014$), and L_p ($p = 0.007$) but decreased E_{glob} ($p = 0.009$) and E_{loc} ($p = 0.039$). No significant between-

Table 2 Global parameters of brain WM structural networks in the patients with non-neuropsychiatric systemic lupus erythematosus (non-NPSLE) and the healthy controls (HC)

Global parameters	Mean ± SD		*p*-value	Cohen *d*
	non-NPSLE	HC		
C_p	0.267 ± 0.01	0.265 ± 0.02	0.406	0.11
L_p	5.085 ± 0.29	4.894 ± 0.22	0.007 ↑	0.74
E_{glob}	0.197 ± 0.01	0.205 ± 0.01	0.009 ↓	0.72
E_{loc}	0.274 ± 0.02	0.282 ± 0.01	0.039 ↓	0.51
σ	3.387 ± 0.22	3.256 ± 0.18	0.019 ↑	0.64
γ	3.694 ± 0.25	3.536 ± 0.22	0.014 ↑	0.66
λ	1.090 ± 0.01	1.086 ± 0.01	0.096	0.38

The arrows (↑ or ↓) indicate significantly increased or decreased parameters in the non-NPSLE patients compared to the controls (10,000 permutations, $p < 0.05$)

Cohen *d* indicates the magnitude of the effect size. The small, medium, and large levels of the effect size are 0.2, 0.5, and 0.8, respectively, according to Cohen's definition (Cohen 1992)

Abbreviations: C_p cluster coefficient, L_p characteristic path length, E_{glob} global efficiency, E_{loc} local efficiency, γ normalized clustering coefficient, λ normalized shortest path length, $\delta = \gamma/\lambda$, *SD* standard deviation

group difference was detected in either C_p ($p = 0.406$) or λ ($p = 0.096$) (10,000 permutations, $p < 0.05$).

Nodal parameters

Figure 2 shows the abnormal brain regions with uniformly significantly decreased nodal efficiency in eight regions in the non-NPSLE patients compared to the controls ($p < 0.05$, FDR corrected). These eight regions are located in the bilateral PreCG, bilateral MFG, bilateral IPL, left median cingulate and paracingulate gyrus (DCG.L), and right middle temporal gyrus (MTG.R) (Table 3). No significant between-group difference survived after an FDR correction in either S_{nod} or *BC*. Table S3 presents the results without FDR correction (Supplementary Materials).

Hub regions

Table 4 lists the hub regions detected in the non-NPSLE patients and the healthy controls. Eight hub regions were found in the patients, while eleven hub regions were found in the controls. Among these hub regions, seven hub regions, including the bilateral precuneus (PCUN.L/R), bilateral putamen (PUT.L/R), PreCG.R, right superior occipital gyrus (SOG.R), and right dorsolateral superior frontal gyrus (SFGdor.R), were the same in the patients and the controls. Four hub regions in the controls, including the right calcarine fissure (CAL.R), PreCG.L, left lingual gyrus (LING.L), and left superior parietal gyrus (SPG.L), were not found in the patients. Finally, a hub region in the left calcarine fissure (CAL.L) was specific to the patients.

Table 3 Brain regions with significantly decreased nodal efficiency (E_{nod}) in the patients with non-neuropsychiatric systemic lupus erythematosus (non-NPSLE) compared to the healthy controls (HC) (10,000 permutations, $p < 0.01$, FDR corrected)

Index	Regions	E_{nod} (mean ± SD)		*p*-value	Cohen *d*
		non-NPSLE	HC		
1	PreCG.L	0.22 ± 0.02	0.23 ± 0.02	3.9e-3 ↓	0.69
2	PreCG.R	0.22 ± 0.02	0.24 ± 0.02	1.1e-3 ↓	0.88
3	MFG.L	0.19 ± 0.02	0.20 ± 0.02	1.1e-3 ↓	0.87
4	MFG.R	0.19 ± 0.02	0.20 ± 0.02	2.2e-3 ↓	0.76
5	IPL.L	0.19 ± 0.01	0.20 ± 0.02	4.1e-3 ↓	0.80
6	IPL.R	0.18 ± 0.01	0.19 ± 0.01	1.7e-3 ↓	0.78
7	DCG.L	0.21 ± 0.02	0.23 ± 0.01	2.2e-3 ↓	0.86
8	MTG.R	0.20 ± 0.02	0.21 ± 0.02	9.0e-4 ↓	0.91

The arrow (↓) indicates significantly decreased nodal efficiency in the non-NPSLE patients compared to the controls

Cohen *d* indicates the magnitude of the effect size. The small, medium, and large levels of the effect size are 0.2, 0.5, and 0.8, respectively, according to Cohen's definition (Cohen 1992)

Abbreviations: *PreCG* precentral gyrus, *MFG* middle frontal gyrus, *IPL* inferior parietal, *DCG* median cingulate and paracingulate gyri, *MTG* middle temporal gyrus, *SD* standard deviation; *L (R)* left (right) hemisphere

Relationships between network parameters and clinical variables

Figure 3 shows the relationships between the nodal efficiency in the abnormal brain regions and the clinical variables in the non-NPSLE patients. In the PreCG.L, the nodal efficiency was significantly negatively correlated with AAO ($r = -0.397$, $p = 0.044$) but positively with DOI ($r = 0.394$, $p = 0.046$). In the MFG.L, the nodal efficiency was significantly negatively correlated with DOP ($r = -0.483$, $p = 0.012$) but positively with C3 ($r = 0.404$, $p = 0.04$) and C4 ($r = 0.428$, $p = 0.029$). The *p*-values for these correlations were not corrected for multiple comparisons. In other brain regions, no such significant correlation was detected in the non-NPSLE patients (Supplementary Materials Table S4).

Abnormal FA, MD, AD, and RD in major WM pathways

Figure 4 shows the WM tract pathways reconstructed using FreeSufer/TRACULA for the non-NPSLE patients and the healthy controls. Compared to the controls, the patients showed significantly increased values of FA and AD in the left CST, significantly increased FA but decreased MD and RD in the right CST, as well as significantly decreased AD in the right SLFT (Table S5 in Supplementary Materials). No significant differences in the diffusion parameters were detected in the bilateral SLFP between the patients and the controls.

Table 4 Hub regions of brain WM structural networks in the patients with non-neuropsychiatric systemic lupus erythematosus (non-NPSLE) and the healthy controls (HC)

non-NPSLE			HC		
Region	Class	E_{nod}	Region	Class	E_{nod}
PCUN.R	Association	0.26	PCUN.R	Association	0.27
PCUN.L	Association	0.26	PCUN.L	Association	0.26
PUT.R	Subcortical	0.24	PUT.R	Subcortical	0.25
PUT.L	Subcortical	0.23	PUT.L	Subcortical	0.24
PreCG.R	Primary	0.22	PreCG.R	Primary	0.24
SOG.R	Association	0.22	SOG.R	Association	0.23
SFGdor.R	Association	0.22	SFGdor.R	Association	0.23
CAL.L	Primary	0.22	CAL.R	Primary	0.23
			PreCG.L	Primary	0.23
			LING.L	Association	0.23
			SPG.L	Association	0.23

The hubs are listed in descending order of nodal efficiency (E_{nod}) for each group. The regions shown in gray are the common hubs found in both groups

Abbreviations: *PCUN* precuneus, *PUT* putamen, *PreCG* precentral gyrus, *SOG* superior occipital gyrus, *SFGdor* dorsolateral superior frontal gyrus, *CAL* calcarine, *LING* lingual gyrus, *SPG* superior parietal gyrus, L (R), left (right) hemisphere

Robustness of the network analysis

Table 5 lists the robustness analysis results for the topological parameters of the brain structural networks in the non-NPSLE patients and the controls when using different definitions of edge weight and nodes. We found that the significantly increased δ, γ, and L_p, as well as the decreased E_{glob} and E_{loc} were highly consistent across different selections of *SN* and different definitions of edge weight. This indicates that the results were highly consistent with the main results derived from $w_{ij} = FA \times SN$ ($SN \geq 2$). In brief, the tendency to find significant between-group differences in

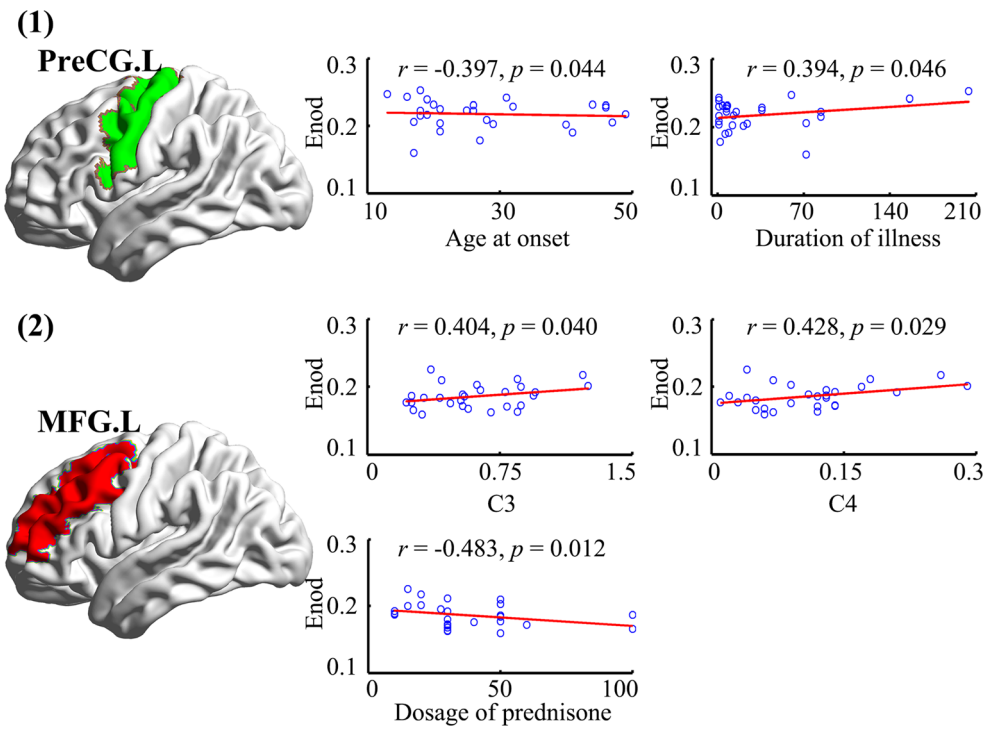

Fig. 3 The relationship between nodal efficiency (E_{nod}) and clinical variables in the patients with non-neuropsychiatric systemic lupus erythematosus (non-NPSLE) compared to the controls. (1) The nodal efficiency of the PreCG.L was significantly negatively correlated with the age at onset (AAO) score but positively correlated with the duration of illness (DOI). (2) The nodal efficiency of the MFG.L was positively correlated with C3 and C4 but negatively correlated with the dosage of prednisone (DOP)

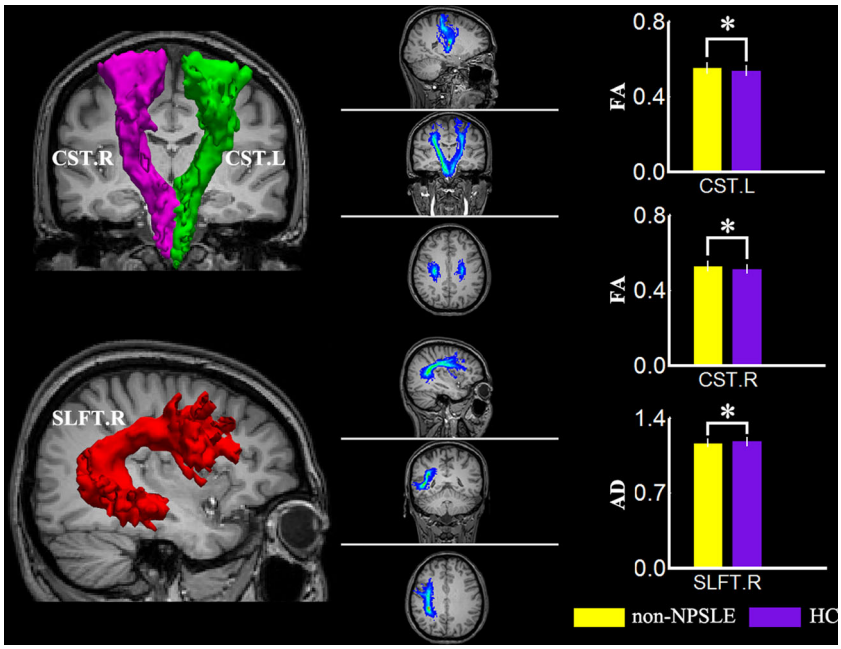

Fig. 4 Brain white matter pathways showing significantly changed diffusion parameters in the patients with non-neuropsychiatric systemic lupus erythematosus (non-NPSLE) compared to the healthy controls (HC). (Left) Corticospinal tract (CST) and superior longitudinal fasciculus–temporal termination (SLFT) pathway; (Middle) Different views of the CST and SLFT; (Right) Fractional anisotropy (FA) and axial diffusivity (AD) in the CST and SLFT pathways. An asterisk indicates a significant difference in either the FA or AD between the non-NPSLE and the controls (10,000 permutations, $p < 0.05$). The images are in radiological orientation

topological parameters was independent of the selections of *SN* and the definitions of edge weight.

The effect of node size on network topology was also tested by using a high-resolution template (AAL-1024) to construct the brain structural networks. We found significant between-group differences in some of the global parameters (significantly changed L_p and marginally significantly changed E_{glob}) in the high-resolution networks (AAL-1024). These results were similar to the results obtained using the AAL-90 template, which we report as the main results. However, we observed that directional changes occurred in the E_{loc}, δ, and γ, depending on the definition of the nodes (Table 5). In addition, the brain regions with significantly decreased E_{nod} in the high-resolution networks (AAL-1024) were highly consistent with

Table 5 The robustness analysis for the topological parameters obtained with different strategies for the patients with non-neuropsychiatric systemic lupus erythematosus (non-NPSLE) compared to the healthy controls (HC)

Network parameters	*p*-value (Cohen *d*)						
	AAL-90						*AAL-1024*
	edge weight			edge weight			edge weight
	$w_{ij} = FA \times SN$			$w_{ij} = SN$			$w_{ij} = FA \times SN$
	$FA \times (SN \geq 1)$	$FA \times (SN \geq 2)$	$FA \times (SN \geq 3)$	$SN \geq 1$	$SN \geq 2$	$SN \geq 3$	$SN \geq 1$
C_p	n.s.	n.s.	n.s.	n.s.	n.s.	n.s.	n.s.
L_p	0.01 (0.6) ↑	0.01 (0.7) ↑	0.01 (0.8) ↑	0.04 (0.5) ↑	0.048 (0.5) ↑	0.045 (0.5) ↑	0.04 (0.5) ↑
E_{glob}	0.02 (0.6) ↓	0.01 (0.7) ↓	0.01 (0.7) ↓	0.06 (0.5) ↓	0.06 (0.5) ↓	0.06 (0.5) ↓	0.06 (0.5) ↓
E_{loc}	0.04 (0.5) ↓	0.04 (0.5) ↓	0.04 (0.5) ↓	n.s.	n.s.	n.s.	n.s.
δ	0.03 (0.5) ↑	0.03 (0.5) ↑	0.02 (0.6) ↑	0.04 (0.5) ↑	0.04 (0.5) ↑	0.02 (0.6) ↑	n.s.
γ	0.04 (0.5) ↑	0.01 (0.7) ↑	0.01 (0.7) ↑	0.01 (0.7) ↑	0.01 (0.7) ↑	0.01 (0.7) ↑	n.s.
λ	n.s.	n.s.	0.04 (0.5) ↑	n.s.	n.s.	n.s.	n.s.

Two types of definitions for the edge weight were utilized in constructing the structural networks: $w_{ij} = FA \times SN$ and $w_{ij} = SN$. The threshold of '$SN \geq 1$, or $SN \geq 2$, or $SN \geq 3$' indicates that two regions were connected if at least 1 or 2 or 3 streamlines exist between a pair of brain regions. One additional high spatial resolution template (AAL-1024) was also used in constructing the structural networks. The arrows (↑ or ↓) indicate significantly increased or decreased parameters in the non-NPSLE patients compared to the controls (10,000 permutations, $p < 0.05$)

Cohen *d* indicates the magnitude of the effect size. The small, medium, and large levels of the effect size are 0.2, 0.5, and 0.8, respectively, according to Cohen's definition (Cohen 1992)

Abbreviations: *FA* fractional anisotropy, SN, streamline number, C_p cluster coefficient, L_p characteristic path length, E_{glob} global efficiency, E_{loc} local efficiency, γ normalized clustering coefficient, λ normalized shortest path length, $\delta = \gamma/\lambda$, *SD* standard deviation, *n.s.* non-significant

those in the low-resolution networks (AAL-90) (Fig. S3 in the Supplementary Materials).

Discussion

In this study, we estimated the topological parameters of brain WM structural network in the non-NPSLE patients and compared them with those of the controls. We found the non-NPSLE patients conserved small-worldness, although the non-NPSLE patients showed significantly decreased E_{glob} and E_{loc} but significantly increased L_p compared to the controls. In addition, the non-NPSLE patients had uniformly significantly decreased nodal efficiency in 8 regions, the bilateral PreCG, bilateral MFG, bilateral IPL, left DCG, and right MTG, compared to the controls. Furthermore, we found abnormal diffusion parameters in the bilateral CST and the right SLFT in the non-NPSLE patients. Taken together, these results may indicate that on a macroscale, the organization of brain WM structural networks has already been changed in SLE patients even in the absence of neuropsychiatric symptoms, which may be induced by abnormal brain WM connectivity.

Global parameters

The small-world properties of a network normally reflect an optimal balance between global integration and local specialization in parallel information processing (Sporns et al. 2000). In this study, the brain WM structural networks for both the non-NPSLE patients and healthy controls showed small-worldness properties ($\gamma >> 1$ and $\lambda \approx 1$, or $\delta >> 1$) (Table 2). However, the non-NPSLE patients showed significantly decreased E_{glob} and E_{loc} but increased L_p compared to the controls (Table 2). Significantly, the changes in these parameters suggest that the global integration and local specialization ability of the parallel information processing may be decreased in the brain WM structural networks in non-NPSLE patients. This result is consistent with a review paper of fMRI findings about SLE patients, in which Mikdashi (2016) indicated that a lack of effective integration and coordination ability among different brain regions was a common phenomenon in SLE patients.

Nodal parameters

Sensorimotor network

We found that the non-NPSLE patients had significantly decreased nodal efficiency in the bilateral PreCG compared to the healthy controls (Table 3 and Fig. 2). The PreCG belongs to the sensorimotor system, which plays an important role in behavioral performance and is a core component of the human brain network (Wang et al. 2013). In fact, previous studies have found abnormal activity in the PreCG in SLE patients (Rocca et al. 2006; Mak et al. 2012; Ren et al. 2012). Our finding of significantly decreased nodal efficiency in the bilateral PreCG also indicates that the abnormal WM connectivity of the PreCG in SLE patients. Interestingly, we found that the nodal efficiency in the PreCG.L was significantly negatively correlated with AAO but positively correlated with DOI in the non-NPSLE patients (Fig. 3). This means that, for the brain WM networks in the non-NPSLE patients, the earlier the onset age or the longer the duration of non-NPSLE illness, the higher the nodal efficiency in the PreCG. This may reflect the brain's adaptability or reorganization in response to the progression of SLE. The significantly increased γ and σ (Table 2) in the non-NPSLE patients compared to the healthy controls may reflect SLE-related plasticity mechanism. This finding is consistent with a previous study (van Meer et al. 2012), which also found significantly increased network parameters (γ and σ) in the sensorimotor network and suggested that this could be related to brain plasticity mechanisms.

The CST conducts impulses from the brain to the spinal cord and is involved in voluntary movement (Wang et al. 2013). Actually, the CST is defined between the primary motor cortex and the midbrain (Wakana et al. 2007). Our result showed significantly increased FA in the bilateral CST in the non-NPSLE patients compared to the controls (Fig. 4). In addition, we found that the non-NPSLE patients had significantly increased AD in the left CST but decreased RD and MD in the right CST compared to the controls (Table S5, Supplementary Materials). Our finding of abnormal diffusion parameters in the bilateral CST in the non-NPSLE patients may suggest that the CST microstructure has been disrupted by SLE even in the absence of neuropsychiatric impairments. We noticed that a previous study (Emmer et al. 2010) reported significantly decreased FA in the CST in NPSLE patients compared to healthy controls when using the TBSS method. The possible reason for this discrepancy, a directional change of FA in the CST, may have resulted from difference in the patient samples or different analytical approaches in the two studies.

Fronto-parietal network

In this study, we found significantly decreased nodal efficiency in the bilateral MFG and IPL in the non-NPSLE patients compared to the healthy controls (Table 3 and Fig. 2). The dorsolateral prefrontal cortex (including the MFG) and posterior parietal cortex (including the IPL and SPL) are important components of the fronto-parietal network (Zanto and Gazzaley 2013). Previous studies suggested that the fronto-parietal network plays an important role in executive control functions, such as working memory, motor planning and execution, cognitive flexibility, inhibition, and abstract reasoning (Astle et al. 2015; Zanto and Gazzaley 2013). Several studies found that SLE patients showed abnormal cognitive function in the fronto-parietal network (Rocca et al. 2006; Fitzgibbon et al.

2008; Hou et al. 2013). Rocca et al. (2006) revealed increased fronto-parietal cortical coactivation compared to healthy controls when NPSLE patients performed a simple motor task. Fitzgibbon et al. (2008) also detected increased fronto-parietal brain activation in NPSLE patients compared to healthy controls when performing working memory tasks via an *n*-back paradigm. In addition, Hou et al. (2013) detected significantly increased frontal-parietal functional connectivity in non-NPSLE patients compared to healthy controls when performing a paced visual serial addition test via a cognitive function task. Thus, our finding of decreased nodal efficiency in the bilateral MFG and IPL may indicate that the fronto-parietal network is disrupted in SLE patients even in the absence of neuropsychiatric symptoms. We also found that the nodal efficiency of the left MFG in the non-NPSLE patients was significantly negatively correlated with DOP but positively correlated with C3 and C4 (Fig. 3). This may indicate the impaired function in the MFG is related to disease severity in SLE.

Fronto-temporal network

The fronto-temporal network plays an important role in mediating cognitive function during working memory tasks, as has been demonstrated in previous studies (Schweitzer et al. 2014; Urbain et al. 2016). Using magnetoencephalography (MEG), Urbain et al. (2016) found desynchronization in the fronto-temporal networks during an *n*-back task in autism spectrum disorder (ASD) patients. In an SLE study, DiFrancesco et al. (2007) also found prefrontal and temporal coactivation in childhood-onset SLE patients when probing working memory performance via the *n*-back paradigm. In this study, in addition to finding significantly decreased E_{nod} in right MFG, we also found that the right MTG had a significantly decreased E_{nod} in the patients compared to the controls (Table 3 and Fig. 2). This suggests that structural damage to the fronto-temporal network in non-NPSLE patients may contribute to cognition dysfunction.

The abnormal function of the fronto-temporal network in SLE patients may be related to impaired WM connectivity. In fact, the SLFT fiber bundle connects the prefrontal and temporal cortices (Wakana et al. 2007). In this study, we found a reduced AD value in the right SLFT in the non-NPSLE patients compared to the controls (Fig. 4), which is consistent with a previous study (Jung et al. 2010). Using a TBSS method, Jung et al. (2010) found a significantly decreased FA in the right SLF in NPSLE patients compared to healthy controls. By analyzing the correlation between the FA and neuropsychological tests, Jung et al. (2012) also found regions with significantly changed FA in the right SLF in NPSLE patients. Thus, these studies paint a picture that impairments in the SLFT cause structural connectivity abnormalities in the fronto-temporal network and may induce further dysfunction in SLE patients.

Hub regions

The altered rich club regions observed in the sensorimotor network and fronto-parietal network may further emphasize the functional impairment in SLE patients. The hub regions detected in the control group are highly consistent with previous DTI studies in healthy adults (Gong et al. 2009; van den Heuvel and Sporns 2011). Of the detected hub regions, seven were common hubs shared by both the patients and controls (Table 4). However, two hub regions, the PreCG.L and SPG.L, belonging respectively to the sensorimotor and fronto-parietal networks, were found in the controls but not in the non-NPSLE patients. Consistent with this hub analysis, we also found significantly decreased E_{nod} in the PreCG (see sensorimotor network heading), which may indicate that the PreCG not only plays a pivotal role in the brain WM structural network but also is vulnerable to damage in non-NPSLE patients. This may be a reason why SLE usually presents as motor function damage (Mikdashi 2016). Previous studies have also found different activation patterns in the SPG when performing different functional tasks (Mak et al. 2012; Hou et al. 2013; Ren et al. 2012). For example, Mak et al. (2012) found less activation in the SPG (BA5/7) in non-NPSLE patients compared to healthy controls when performing executive function tasks. These findings indicate that the functioning of the SPG is also affected by SLE. Taken together, the findings of altered hub regions in brain networks may further suggest that the sensorimotor network and fronto-parietal network are apt to be affected in SLE, even in the absence of neuropsychiatric symptoms.

This study has several limitations. First, we used deterministic tractography to trace the WM tracts to construct WM structural network. Previous studies (Mori and Van Zijl 2002; Jbabdi and Johansen-Berg 2011; Posnansky et al. 2011) have pointed out that deterministic tractography is incapable of resolving crossed or twisted fibers. Probabilistic tractography may be more feasible as it can overcome fiber crossings and is robust to image noise (Behrens et al. 2007). In the future, we will consider using more advanced data reconstruction model, e.g., HARDI for performing fiber tracking. Second, choosing appropriate and precise nodes and edges and identifying the optimal parcellation template to map the brain networks are challenging. Previous studies (Zhong et al. 2015; Zhang et al. 2014) suggested that these factors can affect the reliability of the network analyses. To address these potential issues, we repeated the network analysis using different inter-regional connectivity thresholds and different brain parcellation templates and found that the results showed high robustness (Table 5). Third, when constructing whole-brain WM networks, we did not normalize the volume sizes of

the nodes, even though the volumes of the parcelleted regions are not uniform in the AAL-90 template. In fact, the size of a region may influence the fiber tracking result: a bigger region may have a higher probability of being touched by one of the fiber streamlines (van den Heuvel and Sporns 2011). Actually, previous studies (Andersen et al. 2010; Ripolles et al. 2012) indicated that a volume normalization method may potentially over- or under-compensate for volume-driven effect on the streamline count. And the normalization effect has not been clearly known and this may introduce new confounding factors (van den Heuvel and Sporns 2011). Thus, we choose to focus mainly on the unweighted brain structural network. In addition, to check the robustness of our results, we reconstructed the brain structural networks using a high-resolution brain template (AAL-1024), which parcellates the brain into 1024 regions with equal volumes. The results were similar to those derived from the AAL-90 template (Table 5). Fourth, although we found an abnormal FA value in the CST in the non-NPSLE patients, we cannot infer that the microstructural changes in the CST were caused by the SLE. Several other factors, including myelination, fiber density, axon diameter, cell membrane density, or fiber coherence, may affect the diffusion parameters of WM fibers (Scholz et al. 2009). Fifth, although the AAL template is widely used in constructing WM structural networks in previous studies (Bassett et al. 2011; Lo et al. 2010), it did not included brain WM information as it contains only cortical and subcortical gray matter. In the future, we will consider using more accurate and comprehensive brain templates, such as HCP's multi-modal cortical parcellation atlas (Glasser et al. 2016) or human Brainnetome atlas (Fan et al. 2016), for performing network construction. Finally, the influence of prednisone medication on the brain WM was not considered and may have biased our result. A previous study indicated that medication usage may cause physical structure changes in the brain (Navari and Dazzan 2009). To avoid the effect of this potential factor, a feasible method in the future would be to separate the medication-untreated SLE patients (first-episode and medication-naive patients) from the medication-treated SLE patients to uncover abnormal WM in SLE patients.

In summary, we explored the topological properties of the brain WM structural networks in non-NPSLE patients by using graph theory. The non-NPSLE patients showed several abnormal regions related to sensorimotor and executive control function. Additionally, these patients showed abnormal diffusion properties in the bilateral CST and right SLFT, which are primarily responsible for movement and executive control functions. These results may suggest that altered sensorimotor and executive control function already exist in non-NPSLE patients before the disease evolves to NPSLE. Our findings allow a better understanding of the basis of brain WM structure in non-NPSLE patients and also provide new insights into the pathogenic mechanisms of neuropsychiatric symptoms.

Acknowledgements The authors express their appreciation to Drs. Rhoda E. and Edmund F. Perozzi for editing assistance and thank the two anonymous reviewers for their constructive comments and their suggestions.

Compliance with ethical standards

Funding This work was partly supported by the Department of Medical Imaging Center, Nanfang Hospital, Southern Medical University, and was partly funded by the National Natural Science Foundation of China (Grant numbers: 81471654, 81428013, 81371535, 81271548, and 81271560).

Conflict of interests The authors declare that they have no competing financial interests.

Ethical approval All procedures performed in studies involving human participants were in accordance with the ethical standards of the institutional or national research committee and with the 1964 Helsinki declaration and its later amendments or comparable ethical standards.

Informed consent Informed consent was obtained from all individual participants included in the study.

References

Andersen, S. M., Rapcsak, S. Z., & Beeson, P. M. (2010). Cost function masking during normalization of brains with focal lesions: still a necessity? *NeuroImage, 53*(1), 78–84.

Appenzeller, S., Vasconcelos Faria, A., Li, L. M., Costallat, L. T., & Cendes, F. (2008). Quantitative magnetic resonance imaging analyses and clinical significance of hyperintense white matter lesions in systemic lupus erythematosus patients. *Annals of Neurology, 64*(6), 635–643.

Astle, D. E., Luckhoo, H., Woolrich, M., Kuo, B.-C., Nobre, A. C., & Scerif, G. (2015). The neural dynamics of fronto-parietal networks in childhood revealed using magnetoencephalography. *Cerebral Cortex, 25*(10), 3868–3876.

Bassett, D. S., Brown, J. A., Deshpande, V., Carlson, J. M., & Grafton, S. T. (2011). Conserved and variable architecture of human white matter connectivity. *NeuroImage, 54*(2), 1262–1279.

Behrens, T., Berg, H. J., Jbabdi, S., Rushworth, M., & Woolrich, M. (2007). Probabilistic diffusion tractography with multiple fibre orientations: what can we gain? *NeuroImage, 34*(1), 144–155.

Benedict, R., Shucard, J., Zivadinov, R., & Shucard, D. (2008). Neuropsychological impairment in systemic lupus erythematosus: a comparison with multiple sclerosis. *Neuropsychology Review, 18*(2), 149–166.

Benjamini, Y., & Hochberg, Y. (1995). Controlling the false discovery rate: a practical and powerful approach to multiple testing. *Journal of the Royal Statistical Society. Series B (Methodological), 57*(57), 289–300.

Benner, T., van der Kouwe, A. J., & Sorensen, A. G. (2011). Diffusion imaging with prospective motion correction and reacquisition. *Magnetic Resonance in Medicine, 66*(1), 154–167.

Bombardier, C., Gladman, D. D., Urowitz, M. B., Caron, D., Chang, C. H., Austin, A., et al. (1992). Derivation of the SLEDAI. A disease activity index for lupus patients. *Arthritis and Rheumatism, 35*(6), 630–640.

Brunner, H. I., Feldman, B. M., Bombardier, C., & Silverman, E. D. (1999). Sensitivity of the systemic lupus erythematosus disease activity index, British isles lupus assessment group index, and systemic lupus activity measure in the evaluation of clinical change in childhood-onset systemic lupus erythematosus. *Arthritis and Rheumatism, 42*(7), 1354–1360.

Bullmore, E., & Sporns, O. (2009). Complex brain networks: graph theoretical analysis of structural and functional systems. *Nature Reviews. Neuroscience, 10*(3), 186–198.

Cohen, J. (1992). A power primer. *Psychological Bulletin, 112*(1), 155.

Daianu, M., Mezher, A., Mendez, M. F., Jahanshad, N., Jimenez, E. E., & Thompson, P. M. (2015). Disrupted rich club network in behavioral variant frontotemporal dementia and early-onset Alzheimer's disease. *Human Brain Mapping, 33*, 868–883.

DiFrancesco, M. W., Holland, S. K., Ris, M. D., Adler, C. M., Nelson, S., DelBello, M. P., et al. (2007). Functional magnetic resonance imaging assessment of cognitive function in childhood-onset systemic lupus erythematosus: a pilot study. *Arthritis and Rheumatism, 56*(12), 4151–4163. doi:10.1002/art.23132.

Emmer, B. J., Veer, I. M., Steup-Beekman, G. M., Huizinga, T. W., van der Grond, J., & van Buchem, M. A. (2010). Tract-based spatial statistics on diffusion tensor imaging in systemic lupus erythematosus reveals localized involvement of white matter tracts. *Arthritis and Rheumatism, 62*(12), 3716–3721.

Ercan, E., Magro-Checa, C., Valabregue, R., Branzoli, F., Wood, E. T., Steup-Beekman, G. M., et al. (2016). Glial and axonal changes in systemic lupus erythematosus measured with diffusion of intracellular metabolites. *Brain, 139*(5), 1447–1457.

Fan, L., Li, H., Zhuo, J., Zhang, Y., Wang, J., Chen, L., et al. (2016). The human Brainnetome atlas: a new brain atlas based on connectional architecture. *Cerebral Cortex, 26*(8), 3508–3526.

Filley, C. M., Kozora, E., Brown, M. S., Miller, D. E., West, S. G., Arciniegas, D. B., et al. (2009). White matter microstructure and cognition in non-neuropsychiatric systemic lupus erythematosus. *Cognitive and Behavioral Neurology, 22*(1), 38–44.

Fitzgibbon, B. M., Fairhall, S. L., Kirk, I. J., Kalev-Zylinska, M., Pui, K., Dalbeth, N., et al. (2008). Functional MRI in NPSLE patients reveals increased parietal and frontal brain activation during a working memory task compared with controls. *Rheumatology (Oxford), 47*(1), 50–53. doi:10.1093/rheumatology/kem287.

Fornito, A., Zalesky, A., & Bullmore, E. T. (2010). Network scaling effects in graph analytic studies of human resting-state FMRI data. *Frontiers in Systems Neuroscience, 4*, 22–22.

Gladman, D., Ginzler, E., Goldsmith, C., Fortin, P., Liang, M., Sanchez-Guerrero, J., et al. (1996). The development and initial validation of the systemic lupus international collaborating clinics/American College of Rheumatology damage index for systemic lupus erythematosus. *Arthritis and Rheumatism, 39*(3), 363–369.

Glasser, M. F., Coalson, T. S., Robinson, E. C., Hacker, C. D., Harwell, J., Yacoub, E., et al. (2016). A multi-modal parcellation of human cerebral cortex. *Nature, 536*(7615), 171–178.

Gong, G., He, Y., Concha, L., Lebel, C., Gross, D. W., Evans, A. C., et al. (2009). Mapping anatomical connectivity patterns of human cerebral cortex using in vivo diffusion tensor imaging tractography. *Cerebral Cortex, 19*(3), 524–536. doi:10.1093/cercor/bhn102.

Hochberg, M. C. (1997). Updating the American College of Rheumatology revised criteria for the classification of systemic lupus erythematosus. *Arthritis and Rheumatism, 40*(9), 1725–1725.

Hou, J., Lin, Y., Zhang, W., Song, L., Wu, W., Wang, J., et al. (2013). Abnormalities of frontal-parietal resting-state functional connectivity are related to disease activity in patients with systemic lupus erythematosus. *PloS One, 8*(9), e74530.

Jbabdi, S., & Johansen-Berg, H. (2011). Tractography: where do we go from here? *Brain Connectivity, 1*(3), 169–183.

Jeltsch-David, H., & Muller, S. (2014). Neuropsychiatric systemic lupus erythematosus: pathogenesis and biomarkers. *Nature Reviews. Neurology, 10*(10), 579–596.

Jenkinson, M., Bannister, P., Brady, M., & Smith, S. (2002). Improved optimization for the robust and accurate linear registration and motion correction of brain images. *NeuroImage, 17*(2), 825–841.

Jung, R. E., Caprihan, A., Chavez, R. S., Flores, R. A., Sharrar, J., Qualls, C. R., et al. (2010). Diffusion tensor imaging in neuropsychiatric systemic lupus erythematosus. *BMC Neurology, 10*(1), 65.

Jung, R. E., Chavez, R. S., Flores, R. A., Qualls, C., Sibbitt Jr., W. L., & Roldan, C. A. (2012). White matter correlates of neuropsychological dysfunction in systemic lupus erythematosus. *PloS One, 7*(1), e28373.

Koldewyn, K., Yendiki, A., Weigelt, S., Gweon, H., Julian, J., Richardson, H., et al. (2014). Differences in the right inferior longitudinal fasciculus but no general disruption of white matter tracts in children with autism spectrum disorder. *Proceedings of the National Academy of Sciences of the United States of America, 111*(5), 1981–1986. doi:10.1073/pnas.1324037111.

Kozora, E., Hanly, J. G., Lapteva, L., & Filley, C. M. (2008). Cognitive dysfunction in systemic lupus erythematosus: past, present, and future. *Arthritis and Rheumatism, 58*(11), 3286–3298.

Kozora, E., Brown, M., Filley, C., Zhang, L., Miller, D., West, S., et al. (2011). Memory impairment associated with neurometabolic abnormalities of the hippocampus in patients with non-neuropsychiatric systemic lupus erythematosus. *Lupus, 20*(6), 598–606.

Leemans, A., & Jones, D. K. (2009). The B-matrix must be rotated when correcting for subject motion in DTI data. *Magnetic Resonance in Medicine, 61*(6), 1336–1349.

Li, Y., Jewells, V., Kim, M., Chen, Y., Moon, A., Armao, D., et al. (2013). Diffusion tensor imaging based network analysis detects alterations of neuroconnectivity in patients with clinically early relapsing-remitting multiple sclerosis. *Human Brain Mapping, 34*(12), 3376–3391.

Liang, M., Corzillius, M., Bae, S., Lew, R., Fortin, P., Gordon, C., et al. (1999). The American College of Rheumatology nomenclature and case definitions for neuropsychiatric lupus syndromes. *Arthritis and Rheumatism, 42*(4), 599–608.

Lin, Y., Zou, Q. H., Wang, J., Wang, Y., Zhou, D. Q., Zhang, R. H., et al. (2011). Localization of cerebral functional deficits in patients with non-neuropsychiatric systemic lupus erythematosus. *Human Brain Mapping, 32*(11), 1847–1855. doi:10.1002/hbm.21158.

Lo, C. Y., Wang, P. N., Chou, K. H., Wang, J., He, Y., & Lin, C. P. (2010). Diffusion tensor tractography reveals abnormal topological organization in structural cortical networks in Alzheimer's disease. *The Journal of Neuroscience, 30*(50), 16876–16885. doi:10.1523/JNEUROSCI.4136-10.2010.

Luyendijk, J., Steens, S., Ouwendijk, W., Steup-Beekman, G., Bollen, E., van der Grond, J., et al. (2011). Neuropsychiatric systemic lupus erythematosus: lessons learned from magnetic resonance imaging. *Arthritis and Rheumatism, 63*(3), 722–732.

Mak, A., Ren, T., Fu, E. H., Cheak, A. A., & Ho, R. C. (2012). A prospective functional MRI study for executive function in patients with systemic lupus erythematosus without neuropsychiatric symptoms. *Seminars in Arthritis and Rheumatism, 41*(6), 849–858. doi:10.1016/j.semarthrit.2011.11.010.

Mikdashi, J. A. (2016). Altered functional neuronal activity in neuropsychiatric lupus: a systematic review of the fMRI investigations. *Seminars in Arthritis and Rheumatism, 45*(4), 455–462.

Mori, S., & Van Zijl, P. C. (2002). Fiber tracking: principles and strategies-a technical review. *NMR in Biomedicine, 15*(7–8), 468–480.

Mori, S., & Zhang, J. (2006). Principles of diffusion tensor imaging and its applications to basic neuroscience research. *Neuron, 51*(5), 527–539.

Mori, S., Crain, B. J., Chacko, V., & Van Zijl, P. (1999). Three-dimensional tracking of axonal projections in the brain by magnetic resonance imaging. *Annals of Neurology, 45*(2), 265–269.

Navari, S., & Dazzan, P. (2009). Do antipsychotic drugs affect brain structure? A systematic and critical review of MRI findings. *Psychological Medicine, 39*(11), 1763–1777.

Nichols, T. E., & Holmes, A. P. (2002). Nonparametric permutation tests for functional neuroimaging: a primer with examples. *Human Brain Mapping, 15*(1), 1–25.

Posnansky, O., Kupriyanova, Y., & Shah, N. J. (2011). On the problem of gradient calibration in diffusion weighted imaging. *International Journal of Imaging Systems and Technology, 21*(3), 271–279.

Ren, T., Ho, R. C.-M., & Mak, A. (2012). Dysfunctional cortico-basal ganglia-thalamic circuit and altered hippocampal-amygdala activity on cognitive set-shifting in non-neuropsychiatric systemic lupus erythematosus. *Arthritis and Rheumatism, 64*(12), 4048–4059. doi:10.1002/art.34660.

Ripolles, P., Marco-Pallarés, J., de Diego-Balaguer, R., Miro, J., Falip, M., Juncadella, M., et al. (2012). Analysis of automated methods for spatial normalization of lesioned brains. *NeuroImage, 60*(2), 1296–1306.

Rocca, M. A., Agosta, F., Mezzapesa, D. M., Ciboddo, G., Falini, A., Comi, G., et al. (2006). An fMRI study of the motor system in patients with neuropsychiatric systemic lupus erythematosus. *NeuroImage, 30*(2), 478–484. doi:10.1016/j.neuroimage.2005.09.047.

Rohde, G., Barnett, A., Basser, P., Marenco, S., & Pierpaoli, C. (2004). Comprehensive approach for correction of motion and distortion in diffusion-weighted MRI. *Magnetic Resonance in Medicine, 51*(1), 103–114.

Rubinov, M., & Sporns, O. (2010). Complex network measures of brain connectivity: uses and interpretations. *NeuroImage, 52*(3), 1059–1069. doi:10.1016/j.neuroimage.2009.10.003.

Scholz, J., Klein, M. C., Behrens, T. E., & Johansen-Berg, H. (2009). Training induces changes in white-matter architecture. *Nature Neuroscience, 12*(11), 1370–1371.

Schweitzer, J. B., Faber, T. L., Grafton, S. T., Tune, L. E., Hoffman, J. M., & Kilts, C. D. (2014). Alterations in the functional anatomy of working memory in adult attention deficit hyperactivity disorder. *The American Journal of Psychiatry, 157*(2), 278–280.

Shapira-Lichter, I., Weinstein, M., Lustgarten, N., Ash, E., Litinsky, I., Aloush, V., et al. (2016). Impaired diffusion tensor imaging findings in the corpus callosum and cingulum may underlie impaired learning and memory abilities in systemic lupus erythematosus. *Lupus, 25*(11), 1200–1208.

Shu, N., Liu, Y., Li, K., Duan, Y., Wang, J., Yu, C., et al. (2011). Diffusion tensor tractography reveals disrupted topological efficiency in white matter structural networks in multiple sclerosis. *Cerebral Cortex, 21*(11), 2565–2577.

Sporns, O., Tononi, G., & Edelman, G. M. (2000). Theoretical neuroanatomy: relating anatomical and functional connectivity in graphs and cortical connection matrices. *Cerebral Cortex, 10*(2), 127–141.

Sun, Y., Chen, Y., Collinson, S. L., Bezerianos, A., & Sim, K. (2015). Reduced hemispheric asymmetry of brain anatomical networks is linked to schizophrenia: a connectome study. *Cereb Cortex*, bhv255.

Tzourio-Mazoyer, N., Landeau, B., Papathanassiou, D., Crivello, F., Etard, O., Delcroix, N., et al. (2002). Automated anatomical labeling of activations in SPM using a macroscopic anatomical parcellation of the MNI MRI single-subject brain. *NeuroImage, 15*(1), 273–289.

Urbain, C., Vogan, V. M., Ye, A. X., Pang, E. W., Doesburg, S. M., & Taylor, M. J. (2016). Desynchronization of fronto-temporal networks during working memory processing in autism. *Human Brain Mapping, 37*(1), 153–164.

van den Heuvel, M. P., & Sporns, O. (2011). Rich-club organization of the human connectome. *The Journal of Neuroscience, 31*(44), 15775–15786. doi:10.1523/JNEUROSCI.3539-11.2011.

van Meer, M. P., Otte, W. M., van der Marel, K., Nijboer, C. H., Kavelaars, A., van der Sprenkel, J. W. B., et al. (2012). Extent of bilateral neuronal network reorganization and functional recovery in relation to stroke severity. *The Journal of Neuroscience, 32*(13), 4495–4507.

Wakana, S., Caprihan, A., Panzenboeck, M. M., Fallon, J. H., Perry, M., Gollub, R. L., et al. (2007). Reproducibility of quantitative tractography methods applied to cerebral white matter. *NeuroImage, 36*(3), 630–644. doi:10.1016/j.neuroimage.2007.02.049.

Wang, B., Fan, Y., Lu, M., Li, S., Song, Z., Peng, X., et al. (2013). Brain anatomical networks in world class gymnasts: a DTI tractography study. *NeuroImage, 65*, 476–487.

Wen, W., Zhu, W., He, Y., Kochan, N. A., Reppermund, S., Slavin, M. J., et al. (2011). Discrete neuroanatomical networks are associated with specific cognitive abilities in old age. *The Journal of Neuroscience, 31*(4), 1204–1212.

Yendiki, A., Panneck, P., Srinivasan, P., Stevens, A., Zollei, L., Augustinack, J., et al. (2011). Automated probabilistic reconstruction of white-matter pathways in health and disease using an atlas of the underlying anatomy. *Frontiers in Neuroinformatics, 5*, 23. doi:10.3389/fninf.2011.00023.

Yendiki, A., Koldewyn, K., Kakunoori, S., Kanwisher, N., & Fischl, B. (2013). Spurious group differences due to head motion in a diffusion MRI study. *NeuroImage, 88C*, 79–90. doi:10.1016/j.neuroimage.2013.11.027.

Zalesky, A., Fornito, A., Harding, I. H., Cocchi, L., Yücel, M., Pantelis, C., et al. (2010). Whole-brain anatomical networks: does the choice of nodes matter? *NeuroImage, 50*(3), 970–983.

Zanto, T. P., & Gazzaley, A. (2013). Fronto-parietal network: flexible hub of cognitive control. *Trends in Cognitive Sciences, 17*(12), 602–603.

Zhang, R., Wei, Q., Kang, Z., Zalesky, A., Li, M., Xu, Y., et al. (2014). Disrupted brain anatomical connectivity in medication-naïve patients with first-episode schizophrenia. *Brain Structure & Function, 220*(2), 1145–1159.

Zhong, S., He, Y., & Gong, G. (2015). Convergence and divergence across construction methods for human brain white matter networks: an assessment based on individual differences. *Human Brain Mapping, 36*(5), 1995–2013.

Zimny, A., Szmyrka-Kaczmarek, M., Szewczyk, P., Bladowska, J., Pokryszko-Dragan, A., Gruszka, E., et al. (2014). In vivo evaluation of brain damage in the course of systemic lupus erythematosus using magnetic resonance spectroscopy, perfusion-weighted and diffusion-tensor imaging. *Lupus, 23*(1), 10–19.